

Research Article

Multi-gait snake robot for inspecting inner wall of a pipeline

Jingwei Liu^{a,b}, Man Li^{a,b}, Yahui Wang^{a,b,*}, Da Zhao^a, Rui Deng^a^a School of Electrical and Information Engineering, Beijing University of Civil Engineering and Architecture, Beijing 100044, China^b Beijing Key Laboratory of Robot Bionics and Function Research, Beijing 100044, China

ARTICLE INFO

Article history:

Received 11 November 2023

Revised 10 February 2024

Accepted 27 February 2024

Available online 16 March 2024

Keywords:

Pipeline inner wall detection

Snake robot

Spiral motion

Backbone curve

Modeling and simulation

ABSTRACT

In the field of pipeline inner wall inspection, the snake robot demonstrates significant advantages over other inspection methods. While a simple traveling wave or meandering motion will suffice for inspecting the inner wall of small-diameter pipes, comprehensively and meticulously inspecting the inner wall of large-diameter pipes requires the snake robot to adopt a helical gait that closely adheres to the inner wall. Our review of existing literature indicates that most research and development on the helical gait of snake robots has focused on the outer surface of cylinders, with very few studies dedicated to developing a helical gait specifically for the inspection of the inner wall of pipes. Therefore, in this study, we propose a helical gait that is suitable for the inner wall of pipes and meets the requirements of gas pipeline engineering. The helical gait is designed using the backbone curve method. First, we create a mathematical model for a circular helix curve with constant curvature and torsion, ensuring it is applicable to a snake robot prototype in a laboratory environment. Subsequently, we calculate the joint angles required for two conical spiral curves with variable curvature and torsion, establish a new model, and define the physical significance of the specific parameters. To ensure the feasibility of the proposed gait, we conduct experiments involving meandering and traveling wave motions to verify the communication and control between the host computer and the snake robot. Building upon this foundation, we further validate the mathematical model of the complex helical motion gait through simulation experiments. Our findings provide a theoretical basis for realizing helical movement with a real snake robot.

© 2024 The Author(s). Published by Elsevier B.V. on behalf of Shandong University. This is an open access article under the CC BY-NC-ND license (<http://creativecommons.org/licenses/by-nc-nd/4.0/>).

1. Introduction

Pipeline transportation has been embraced across a diverse range of sectors, including oil, gas, water supply, drainage, and heating systems. Despite their widespread use, pipelines remain vulnerable to environmental factors. These vulnerabilities can lead to potential impairments such as cracks and other defects, which, if not promptly addressed, can culminate in catastrophic incidents. Therefore, it is imperative to routinely inspect and maintain the internal structure of pipelines. Unfortunately, existing inspection methodologies often fail to determine the precise coordinates and orientations of pipeline leaks, resulting in substantial safety concerns [1,2].

In response to these challenges, researchers have proposed the deployment of pipeline robots as an effective and precise inspection solution. Nevertheless, the majority of pipeline robot designs cater to larger pipe diameters, primarily adopting a wheel or track system, with minimal research and development focused on creating robots suitable for small to large pipe diameters. To

fill this research gap, Rui et al. [3], from our research group, conceived and developed a specialized snake robot for inspecting the inner surfaces of pipelines. This pioneering robot is composed of multiple orthogonally interconnected joint modules that facilitate fundamental motion patterns such as meandering movements and traveling waves within the pipeline.

In the study of locomotion gait for snake robots, fitting different curve shapes results in various crawling effects. Researchers have made notable progress in establishing effective motion patterns. For two-dimensional motion, undulatory motion is recognized as a highly efficient gait and has been the focus of extensive research. Hirose et al. [4], through experiments on and observations of biological snakes, proposed the Serpenoid curve to model undulatory motion. Ma et al. [5] introduced the Serpentine curve, demonstrating from a motion efficiency perspective that this curve provides a superior fit compared with the Serpenoid curve.

The three-dimensional gaits of snake robots mainly encompass lateral shifting, climbing, and other movements characterized by helical curves. For snake robots with discrete structures, the generation of three-dimensional movement gaits typically involves fitting helical curves using gait equations and the backbone

* Corresponding author.

E-mail address: yahui-wang@vip.sina.com (Y. Wang).

curve method to produce the robot's three-dimensional motion patterns [6].

The gait equation approach assigns each joint of the robot to a parameterized equation, with the joint angles described as a function of time and number of joints. Hirose et al. [4] simplified and fitted the Serpenoid curve to derive the gait equations for the undulatory gait of snake robots. Subsequently, various movements, such as circular and lateral wrapping, were created using gait equations [7,8]. However, for complex motion shapes, it is challenging to establish direct control equations using the gait equation method.

To generate three-dimensional gaits, Liljebäck et al. [9] employed the D-H method, systematically describing the kinematics of snake robots based on recursive algorithms. For more intricate three-dimensional gaits, Burdick et al. [10] used the Frenet-Serret formula and introduced the backbone curve method, which enabled the desired robot shape to be extrapolated using a continuous backbone curve. Yamada et al. [11] proposed a model that considered the robot's joint structure, which simplified the fitting process. Andersson et al. [12] and Liljebäck et al. [13] employed the backbone curve method to generate the joint angles of snake robots corresponding to the curvature and torsion of spatial curves, allowing for the construction of more complex motion patterns. Chong et al. [14] focused on modeling the "S" shaped curve and described the helical side-shifting motion. Huang et al. [15], using the backbone curve method, established an ideal mathematical model for helical motion on a cylindrical surface and applied this model to climbing movement on cylinder exteriors. Zhen et al. [16] analyzed the gait equations and backbone curve methods for spiral motion in detail, clarifying the relationship between their parameters and proving a certain equivalence between the two approaches.

When deploying snake robots for internal pipeline inspection tasks, basic locomotion gaits, such as traveling waves or undulatory motion, are applicable to small-diameter pipes. However, for large-diameter pipes, a comprehensive inspection of the inner wall necessitates the design of a three-dimensional helical curve motion gait that causes the snake robot to support itself against the pipe's inner surface. Tanaka et al. [17] proposed a unified motion method for snake robots traversing complex structures inside pipelines, including a shifting motion method for navigating various obstacles. They also proposed a motion method for changes in pipeline diameter and a motion method for movement between the inside and outside of a pipe. A major difference between this study and our study is that our study focuses on the urban underground pipeline system, which is mainly composed of gas pipelines. Most underground gas pipelines are straight pipes of different sizes. The key challenge addressed by our study is that any snake robot deployed in gas pipelines in engineering applications must be equipped with various sensors, and its motion must adapt to different inspection tasks. When confirming the presence of sediment or cracks in a pipeline during the testing phase, it is necessary to clear the sediment or patch cracks in the inner wall. It is planned that in the future, the head can be replaced with a reamer or special tools for patching cracks. Therefore, the snake robot that we develop must exhibit sufficient mechanical strength and power to complete these tasks, which explains the relatively large size of our snake robot. Overall, our snake robot is specialized, whereas Tanaka's snake robot exhibits a universal motion gait.

In this study, considering the context of pipeline applications, we focus on the modeling and simulation analysis of helical motion for snake robots during horizontal straight pipeline inner wall inspections, which includes clarifying the physical significance of specific parameters in the modeling process. We demonstrate that cylindrical spiral motion causes the head camera to

Table 1
Comparison of snake robot structures.

Structural	Feature
Active wheel	Low friction, Simple structure, Suitable for Serpentine motion
Passive wheel	High degree of freedom and flexibility, Complex joint coordination control
Crawler-type	Large contact area, Able to adapt to unstructured confined spaces
Other types	Relying on oneself and the external environment to generate driving force

closely adhere to the pipe wall, resulting in a limited inspection space, and the robot's overall support on the inner side of the pipe wall leads to a slower travel speed. To solve the practical challenges encountered by snake-shaped robots during pipeline inner wall inspection tasks, we suggest the use of conical spiral motion within the pipeline. The main contributions of this study are as follows:

(1) The snake robot prototype developed in this study features orthogonally interconnected joint modules. These modules generate propulsion through friction between their outer skin and the pipeline's inner wall. The robot's head joint is equipped with cameras and sensors to perform the inspection task.

(2) We establish a two-dimensional serpentine curve motion using the gait equation method. We then improve the snake robot's helical motion model based on the backbone curve approach, generate control functions for the joint angles of complex three-dimensional helical curves, and clarify the physical meanings of specific parameters.

(3) To overcome the practical limitations of cylindrical spiral motion in pipeline inspection engineering, we propose the use of conical spiral motion. This motion enables part of the snake robot to leave the inner wall of the pipeline, which is advantageous for pipeline inspection.

(4) Physical experiments validate the feasibility of traveling wave motions. Software simulations in Adams verify the viability of two helical motion gaits, namely cylindrical and conical spiral gaits, thus providing a theoretical foundation for the implementation of helical gaits in subsequent physical snake robots.

2. Structural of snake robot

To enhance the reliability of movement and reduce the development costs of the robot, a simple mechanical structure is prerequisite for the development of a snake robot [18,19].

2.1. Connection method

Snake robots typically possess modular mechanical structures, meaning they are composed of multiple identical or similar modules based on specific functional needs [20]. These structures can be categorized into four types based on their different motion principles: passive wheel structure, active wheel structure, caterpillar structure, and other types of structures. Extensive research has been conducted to assess the pros and cons of each structure, as outlined in Table 1.

Based on the application scenario of inspecting the interior of a gas pipeline, to prevent the risk of a wheel dropping, we rule out wheeled structures. Caterpillar structures are mostly used in the field of rescue in rugged environments.

2.2. Joint module

The snake robot prototype described in this study consists of 21 joint modules. These modules are designed to facilitate

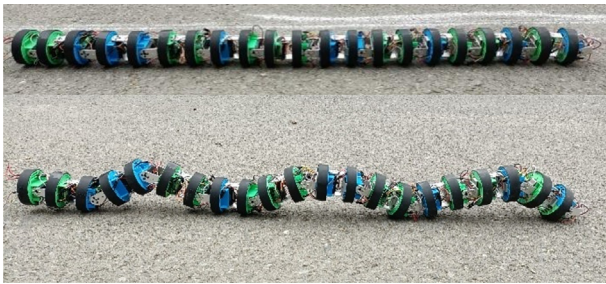


Fig. 1. Snake robot prototype.

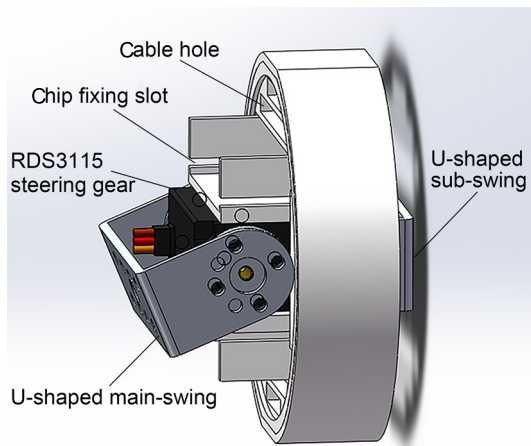


Fig. 2. Joint module.



Fig. 3. Snake robot head's 3D-printed housing for mounting binocular camera (without shield).

The snake body shell is designed with a cylindrical shape to maximize contact with the inner wall of the pipe during the robot's 3D helical movement. Furthermore, because the snake robot is capable of both spiral movement along the inner wall of the pipe and simple linear traveling wave movement, a special plane design is implemented along the vertical direction of the snake robot body. To protect the robot from internal and external factors in the pipeline, a bolt structure secures the shell parts. The shell is also designed to accommodate the control chip and power supply voltage regulator module and facilitate wire connection between modules, with corresponding holes provided on the shell.

The joint shell of the snake robot is made of acrylonitrile butadiene styrene (ABS), which is known for its robust mechanical properties, excellent wear resistance, low water absorption, moderate strength, and compatibility with other materials. The use of ABS ensures that the snake robot can move freely without damage and allows for easy attachment of skin materials to the surface of the shell.

Through extensive experimentation and evaluation of various friction materials, we determine that soft silicone rubber is the most suitable material for the outer skin of the snake robot shell. This material has high wear resistance and provides stable friction. Adhering this silicone rubber onto the surface of the shell ensures direct contact with the inner wall of the pipeline, thereby meeting both requirements for optimal performance. Our findings are summarized in Table 2.

Finally, the outer casing of the snake robot head must be specifically engineered to fulfill the objective of inspecting the inner wall of the pipeline. As depicted in Fig. 3, the head is outfitted with cameras, supplemental lighting, and corresponding sensors to gather real-time images and inspection data within the pipeline. The binocular camera carried by the head of the snake robot can capture images of the inner wall of the pipeline; Fig. 4 shows that the camera can clearly photograph the defects, scratches, and other conditions on the inner wall of the pipeline. At this point, the overall structural design of the snake robot prototype for laboratory testing is complete.

3. Method and modeling

Fig. 5 presents a diagram of a snake robot with joints connected orthogonally. Joints are designated as odd joints if they have odd numbers and as even joints if they have even numbers. Odd joints control the pitch of the snake robot, and even joints control the yaw.

three-dimensional spiral motion within gas pipelines of varying diameters (ranging from 200 mm to 500 mm). Each joint is connected orthogonally along the central axis of the robot. The joints are divided into odd and even joints, allowing for control over the pitch and yaw of the snake robot prototype, respectively. Fig. 1 illustrates the snake robot prototype executing a traveling wave motion on a horizontal concrete surface.

To successfully accomplish the spiral motion along the inner wall of the gas pipeline and effectively perform the inspection task, the joint modules of the snake robot must satisfy the following conditions:

- (1) Implementation of a high-torque steering mechanism is essential to deliver sufficient torque to maintain the desired angular output and meet the power requirements of intricate movements.
- (2) The joint connections must possess adequate structural integrity to ensure that their load-bearing capacity and rigid strength are sufficient to withstand the forces generated during the motion of the snake robot.
- (3) The overall shape of the robot is determined by the shell structure. The outer surface, after the application of skin material, should increase the contact area with the inner wall of the pipeline. This will help ensure the stability of the three-dimensional spiral movement.
- (4) The snake robot relies on the outer skin material of the joint shell to generate friction with the pipe's interior, so the outer skin material should exhibit characteristics such as a high friction coefficient, soft contact, and wear resistance [21].
- (5) The snake head shell structure must incorporate cameras and related sensors to facilitate real-time collection of images and inspection data within the pipe.

Fig. 2 shows that a single joint module consists of five components: a cable hole, a chip fixing slot, a high-torque digital steering gear, a U-shaped main swing, and a U-shaped subswing.

Table 2
The properties of common friction materials.

Properties	Natural rubber	Nitrile butadiene rubber	Silicone rubber
Abrasion resistance	Good	Excellent	Good
Resistant to natural aging	Poor	Medium	Excellent
Antioxidant properties	Good	Medium	Excellent
Heat resistance	Good	Good	Excellent
Compression deformation	Medium	Good	Excellent

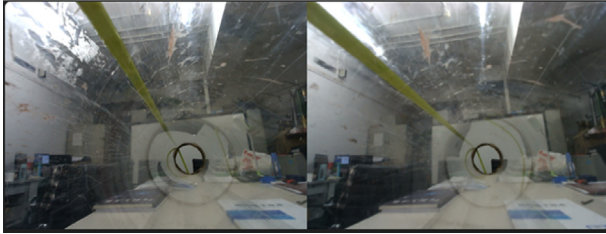


Fig. 4. Screenshot of a snake robot with binocular cameras at rest.

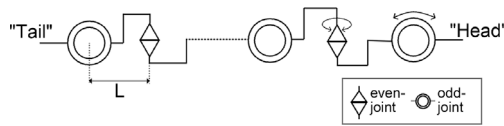


Fig. 5. Snake robot joint connection.

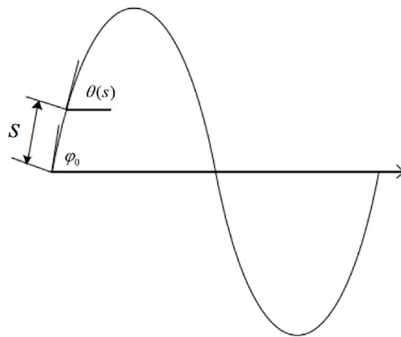


Fig. 6. Serpenoid curve simplified diagram.

3.1. Meandering and traveling gait

The two most commonly observed fundamental locomotion patterns of snake robots are meandering and traveling wave gaits. These gaits are usually employed when robots need to navigate through small-diameter pipelines for pipeline inspection. During movement, the robot adopts a Serpenoid curve shape.

The control function for the serpentine and traveling wave gaits is initially derived from the simplification and fitting of the Serpenoid curve. A simplified diagram of the Serpenoid curve is shown in Fig. 6, and its curvature equation is given as follows [22]:

$$\rho(s) = \frac{2K_n\pi\varphi_0}{nL} \sin\left(\frac{2K_n\pi}{nL}s\right) \quad (1)$$

where K_n is the number of sinusoidal waveforms of the Serpenoid curve, φ_0 is the initial bending angle of the curve, L is the length of one joint of the snake robot, n is the number of joints of the snake robot, and s is the arc length of the curve.

To simplify the calculation, the above curvature expression becomes:

$$\rho(s) = -ab \sin(bs) \quad (2)$$

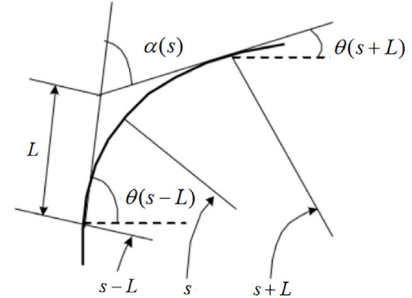


Fig. 7. Schematic diagram of joint angle.

where $a = -\varphi_0$ and $b = \frac{2K_n\pi}{nL}$. The equation for the angle of rotation of a joint moving along a serpentine curve can be obtained by integrating Eq. (2) with respect to the curvature s :

$$\theta(s) = \int -ab \sin(bs) = a \cos(bs) \quad (3)$$

Since the Serpenoid curve is a two-dimensional curve, it is crucial to maintain a value of zero for odd or even joints while moving along the curve. Eq. (4) provides the relationship for calculating the rotation angle between two adjacent isotropic joints. A schematic diagram for this is depicted in Fig. 7.

$$\begin{aligned} \alpha(s) &= \theta(s+L) - \theta(s-L) \\ &= -2a \sin(bL) \cdot \sin(bL) \end{aligned} \quad (4)$$

The gait control function for the Serpenoid curve is generated by replacing Eq. (4) with a function of time for each neighboring isotropic joint:

$$\alpha_i(t) = N \sin(\omega t + Zi) \quad (5)$$

where $N = -2a \sin(bL)$, $\omega t = bs$, and $Z = 2bL$. When the odd joints maintain a value of zero and the middle position remains unchanged, the yaw of the even joints is controlled by the gait equation from Eq. (5). This allows the snake robot to execute a meandering motion on the horizontal plane. Alternatively, if the even joints remain unchanged, it is possible to achieve a traveling wave motion in the vertical plane.

The above process involves generating simple gait equations for meandering and traveling wave motions based on Serpenoid curves. However, it is challenging to establish a suitable equation for complex three-dimensional spiral curves. In such cases, the backbone curve method can be used to calculate the corresponding rotation angle for each joint.

3.2. Backbone curves

Currently, the locomotion of snake robots involves climbing the exterior of a cylinder using either a rolling or spiral-like motion. In the next step of this study, a novel three-dimensional spiral motion model of the inner wall of a pipe is established based on the three-dimensional spiral motion of the outer surface of the cylinder. This is achieved by employing the backbone curve

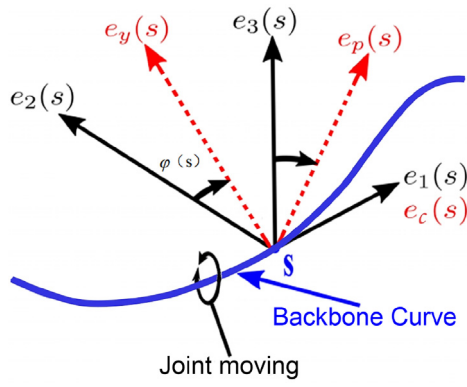


Fig. 8. Backbone curve method.

method to calculate the corresponding joint angles of the steering gear.

To represent the motion profile of a redundant robot, Chirikjian et al. [23] introduced the concept of a backbone curve (Fig. 8).

The backbone curve approach relies on three fundamental orthonormal unit vectors and employs two curve parameters—curvature $k(s)$ and torsion $\tau(s)$ —to mathematically describe the curve in terms of radians s . The first unit vector $e_1(s)$ aligns with the tangent direction of the curve, the second unit vector $e_2(s)$ corresponds to the bending direction of the curve, and the third unit vector $e_3(s)$ is perpendicular to the plane of two vectors ($e_1(s), e_2(s)$). The snake robot's joints are attached to the main curve using various techniques, but this method leads to complex calculations. To simplify the calculations, Yamada et al. [24] introduced a new set of vectors $[e_c, e_y, e_p]$ to describe the motion curve. The vector $e_c(s)$ aligns with $e_1(s)$, $e_y(s)$ points toward the axis of even joints, and $e_p(s)$ points toward the axis of odd joints. The curvature $k(s)$ of the robot's main curve is decomposed, where $k_p(s)$ represents the overall pitch curvature of the snake robot and $k_y(s)$ represents the yaw curvature:

$$k_p(s) = k(s) \sin \varphi(s) \quad (6)$$

$$k_y(s) = k(s) \cos \varphi(s) \quad (7)$$

where $\varphi(s)$ is the angle of torsion between $[e_c, e_y, e_p]$ and $[e_1, e_2, e_3]$.

$$\varphi(s) = \int_0^s \tau(s) ds + \varphi_0 \quad (8)$$

where φ_0 is a constant of integration used to adjust the initial angular offset, and $\tau(s)$ is the torsion around the backbone curve. When the parameter $\varphi(s)$ changes over time, the snake robot is capable of generating movement along the backbone.

3.3. Joint angle

To achieve precise control of the motion shape of the discretely structured snake robot and create a smooth and continuous motion curve along the backbone curve, it is essential to calculate the rotation angle of each joint. The rotation angles of the odd joints can be determined by integrating the pitch curvature k_p over the length of the joints, whereas the rotation angles of the even joints can be obtained by integrating the yaw curvature k_y over the length of the joints. The joint angle of the i th joint is:

$$\alpha_i = \int_{(i-1)L}^{(i+1)L} k_p(s) ds \quad \text{odd joint} \quad (9)$$

$$\alpha_i = \int_{(i-1)L}^{(i+1)L} k_y(s) ds \quad \text{even joint} \quad (10)$$

where L is the length between two neighboring joints and i is the serial number of the joints. After incorporating a time parameter $\alpha_i(t)$ and expressing the joint angles as a function of time, it is possible to generate motion along the backbone curve. Consequently, the pitch curvature, yaw curvature, and torsion angle vary with time. We define the torsional component:

$$T(s) = \int_0^s \tau(s) ds \quad (11)$$

Then we substitute Eq. (11) into Eq. (8) and back into Eq. (7):

$$\begin{aligned} k_y(s, t) &= k(s) \cos(\varphi_0(t) + T(s)) \\ &= k(s) \cdot [\cos \varphi_0(t) \cos T(s) - \sin \varphi_0(t) \sin T(s)] \\ &= \cos \varphi_0(t) K_{\cos} - \sin \varphi_0(t) K_{\sin} \end{aligned} \quad (12)$$

In order to simplify the calculations, we make $k(s) \sin T(s) = K_{\sin}$ and $k(s) \cos T(s) = K_{\cos}$. Then we substitute Eq. (12) into Eq. (10), which yields the formula for the joint angle of odd joints:

$$\begin{aligned} \alpha_i(t) &= \int_{(i-1)L}^{(i+1)L} k_y(s, t) ds \\ &= \cos \varphi_0(t) \alpha_{\cos} - \sin \varphi_0(t) \alpha_{\sin} \end{aligned} \quad (13)$$

where $\alpha_{\cos} = \int_{(i-1)L}^{(i+1)L} K_{\cos}(s) ds$, $\alpha_{\sin} = \int_{(i-1)L}^{(i+1)L} K_{\sin}(s) ds$. Similarly, the joint angle of even joints is obtained as a function of time:

$$\alpha_i(t) = \cos \varphi_0(t) \alpha_{\sin} + \sin \varphi_0(t) \alpha_{\cos} \quad (14)$$

As illustrated in Eqs. (13) and (14), once the values of α_{\sin} and α_{\cos} are established, the joint angles can be calculated over a specific time period. The values of α_{\sin} and α_{\cos} are essentially influenced by the pitch and yaw curvatures. Therefore, when the curvatures and torsion of the backbone curve, which correspond to the pitch and yaw curvatures, are determined, it becomes feasible to compute the variation in joint angles $\alpha_i(t)$ resulting from motion along the backbone curve.

3.4. Cylindrical helical gait

When the backbone curve takes the form of a cylindrical helix, it is possible to compute the angle function of each joint as a function of time, which makes it possible to control the snake robot's motion to follow a corresponding cylindrical helix trajectory. The parametric equation for a general cylindrical helix curve is given by

$$\begin{cases} x = r \cos \theta \\ y = r \sin \theta \\ z = \frac{h}{2\pi} \theta \end{cases} \quad (15)$$

As shown in Fig. 9, h is the displacement distance along the axis of a moving point on a cylindrical helix rotated by one week, which is called the pitch, and r is the radius of the cylindrical helix. The curvature and torsion of the cylindrical helix are

$$k(s) = \frac{r}{r^2 + (\frac{h}{2\pi})^2} \quad (16)$$

$$\tau(s) = \frac{\frac{h}{2\pi}}{r^2 + (\frac{h}{2\pi})^2} \quad (17)$$

According to Eqs. (16) and (17), the curvature k and torsion n are constant values; thus, they are represented as k_0 and τ_0 , respectively. These values are then substituted into Eq. (13), resulting in the following expression:

$$\begin{aligned} \alpha_{\cos} &= \int_{(i-1)L}^{(i+1)L} K_{\cos}(s) ds \\ &= \frac{k_0}{\tau_0} \cdot [\sin(\tau_0(i+1)L) - \sin(\tau_0(i-1)L)] \\ &= \frac{2k_0}{\tau_0} \cdot \sin(\tau_0 L) \cos(\tau_0 Li) \end{aligned} \quad (18)$$

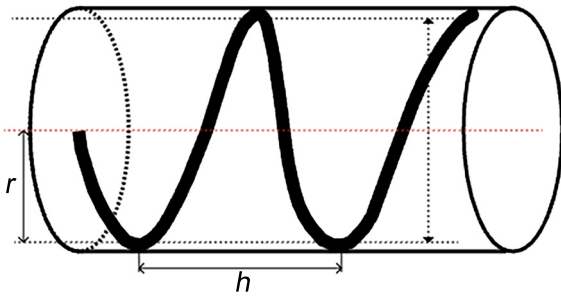


Fig. 9. Cylindrical helical curve.

$$\alpha_{\cos} = -\frac{2k_0}{\tau_0} \cdot \sin(\tau_0 L) \sin(\tau_0 Li) \quad (19)$$

We let $N = \frac{2k_0}{\tau_0} \cdot \sin(\tau_0 L)$ and $Z = \tau_0 L$. By substituting these expressions into Eq. (9), we obtain the relationship between time and the angle of the odd joints during cylindrical helix motion:

$$\begin{aligned} \alpha_i(t) &= N \cdot [\cos \varphi_0(t) \cos(Zi)] \\ &= N \cdot \cos(\omega t - Zi) \end{aligned} \quad (20)$$

where $\omega t = \varphi_0(t)$.

Similarly, joint angles for even joints are

$$\alpha_i(t) = N \cdot \sin(\omega t - Zi) \quad (21)$$

3.5. Conical spiral gait

In this section, we present three-dimensional conical curves with unique spiral motion. While exploring inside the pipe, the movement of the snake robot can be divided into two distinct parts. The first part involves a cylindrical spiral motion that supports the snake body, and the second part involves a conical spiral motion away from the tube wall. By performing conical spiral movements, the snake robot can detach a portion of itself from the tube wall, which allows it a certain level of freedom and mobility. Moreover, this motion enables the head joint of the snake robot to be positioned closer to the center line, theoretically enhancing its ability to capture panoramic video images in front of the pipeline. In addition, by adjusting the parameters, the snake robot can be made to perform special spiral movements wherein it detaches and then reattaches to the pipe wall, thereby achieving a higher travel speed.

Common conical spirals are categorized as conical spirals with equal helix angles (referred to as equal-angle conical spirals) and equal-pitch conical spirals. For convenience of calculation, the expression for an equal-angle conical spiral is defined [25]:

$$\begin{cases} x = ae^{m\theta} \cos \theta \\ y = ae^{m\theta} \sin \theta \\ z = be^{m\theta} \end{cases} \quad (22)$$

The parameters in Eq. (22) are shown in Fig. 10, where $a = n \sin \alpha$ is the rate of change in the radius of the helix, $b = n \cos \alpha$ is the rate at which the z-axis of the helix increases, n is constant, and $m = \sin \alpha \sin \beta$, where α is the conical half vertex angle, and β is the helix angle of the conical spiral.

The curvature and torsion of the conical spiral can be determined by applying the following curvature and torsion formulas:

$$k_1(s) = e^{-m\theta} \sqrt{\frac{2a^2b^2(m^4 + m^2 + 1)}{(a^2 + a^2m^2 + b^2m^2)^3}} \quad (23)$$

$$\tau_1(s) = \frac{1}{m\sqrt{(a^2 + b^2)}} e^{-m\theta} \quad (24)$$

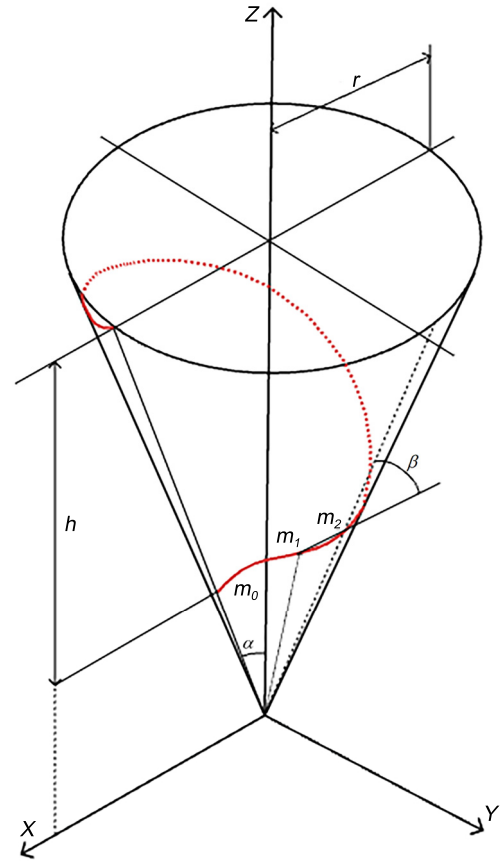


Fig. 10. Conical spiral curve. (The mobile point m begins at m_0 on the conical surface and travels through m_1 and m_2 .)

Next, the parametric equation for a conical spiral with constant pitch variation is

$$\begin{cases} x = a \cdot \theta \cdot \cos \theta \\ y = a \cdot \theta \cdot \sin \theta \\ z = b \cdot \theta \end{cases} \quad (25)$$

where $a = \frac{h}{2\pi} \sin \alpha$, $b = \frac{h}{2\pi} \cos \alpha$, α is the conical half vertex angle, and h is the pitch. The parameters are displayed in Fig. 10. The curvature and torsion of the equal-pitch conical spiral are calculated:

$$k_2(s) = \sqrt{\frac{a^4(\theta^2 + 2)^2 + a^2b^2(\theta^2 + 4)}{[a^2(\theta^2 + 1) + b^2]^3}} \quad (26)$$

$$\tau_2(s) = \frac{b(\theta^2 + 6)}{a^2(\theta^2 + 2)^2 + b^2(\theta^2 + 2) + b^2} \quad (27)$$

The curvature and torsion of a conical spiral both change with the variation of θ . Hence, it is essential to compute the correlation between θ and the arc length of the two conical spirals. The equal-angle conical spiral is

$$\left(\frac{ds}{d\theta}\right)_1 = \sqrt{a^2(\theta^2 - 2\theta \cdot \sin 2\theta + 1) + b^2} \quad (28)$$

The equal-pitch conical spiral is

$$\left(\frac{ds}{d\theta}\right)_2 = m\sqrt{2a^2 + b^2} \cdot e^{m\theta} \quad (29)$$

In summary, after substituting the curvature and torsion values of the three-dimensional conical spiral into Eqs. (9) and (10),

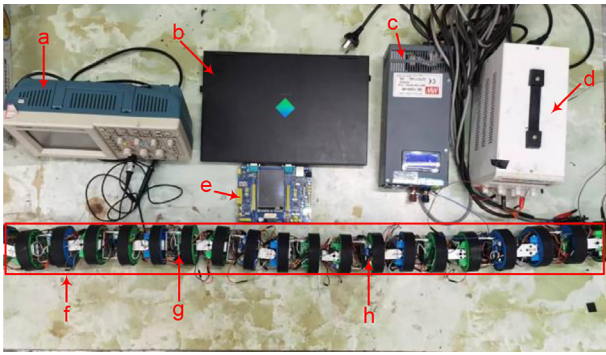


Fig. 11. Test-bed. (a) Oscilloscope (b) PC. (c) 7 V DC power supply. (d) 5 V DC power supply. (e) Main controller. (f) Snake robot prototype. (g) Slave controller. (h) Voltage module.

the resulting joint angle can be determined, as shown in Eq. (30). This finalizes the calculation of the joint angle control function for the conical spiral curve gait.

$$\alpha_i(t) = N(\theta) \cdot \sin(\omega t - Z(\theta) \cdot i) \quad (30)$$

Our modeling method is not exclusively applicable to conical spiral curves; it also provides significant guidance for other intricate three-dimensional curves with varying curvature and torsion.

4. Experiment

4.1. Physical experiment

4.1.1. Experiment platform

List of experimental platforms: prototype of a pipeline inspection snake robot (including a slave controller and power supply regulator module), snake robot upper computer (laptop and main controller), DC power supply, oscilloscope, multimeter, 300 mm diameter transparent organic pipeline, and several cables. Based on a pipeline diameter of 300 mm, the experimental prototype of the snake robot consists of 21 orthogonally interconnected joint modules. Each joint measures 61.5 mm in length and 84 mm in diameter, culminating in a total length of 1291.5 mm for the entire assembly.

Fig. 11 presents the experimental test platform constructed in the laboratory setting. Fig. 12 provides an overview of the control method used in the experiment.

As mentioned above, a regulated power supply with a DC voltage of 36 V is used to supply power to the snake robot. In addition, a DC-regulated voltage conversion module is implemented on the body of the snake robot to convert the voltage from 36 V to 7 V for the joint steering gear and from 36 V to 5 V for the slave controller. The laptop communicates with the master controller via a USB connection, whereas the master and slave controllers are connected using twisted pair cables and communicate through a CAN bus. The input parameters from the upper computer are used to calculate the angle of each joint, and different signals are then sent to the slave controller to control the snake robot. Finally, a pulse-width modulation wave is output from the controller to control the steering gear of the snake robot.

Furthermore, we choose a 36 V DC power supply based on the overall power consumption and current needs of the entire snake robot. The rated power of the servos used is approximately 15 W with a current of 2.2 A. If a 7 V DC power supply on the ground were to uniformly deliver power to all servos and other devices of the subterranean robot, it would necessitate an electrical cable with a large cross-sectional area. The bulk of such cables could

hinder the robot's movements. Therefore, we opt for a safe 36 V DC power source on the ground, which adequately meets the power requirements of the subterranean robot under acceptable cable diameter conditions. After the power cables are connected to the robot, subsequent voltage conversions are applied depending on the voltage requirements of the different components, thereby ensuring sufficient power supply to all electrical devices.

4.1.2. Traveling wave

Within the framework of Eq. (5), the traveling wave gait equation, maintaining a constant value of N while increasing Z leads to a greater wavelength and a reduced number of wave peaks for undulatory motion. In contrast, when Z is held constant, a larger value of N results in an increased amplitude of undulatory movement. The experiment for traveling wave motion within a transparent pipeline is conducted as follows. Parameters are calculated based on actual conditions, and $N = 1.6$ and $Z = 0.4$ are used as the final control parameters. The resulting motion is depicted in Fig. 13.

According to the observation in Fig. 13, the snake robot exhibits a Serpenoid curve motion in the vertical plane, which is well suited for moving through narrow pipes. Using a ruler placed on the transparent pipe, it is determined that the snake robot moves 931.2 mm in the pipe within 68 s. Therefore, based on the given environment and parameters, the average velocity of the snake robot's traveling wave motion is approximately 13.7 mm/s. In addition, the figure reveals a slight sideways movement of the snake robot, which can be attributed to the smooth inner surface of the transparent plexiglass pipe in the laboratory environment. In future engineering environments, an increase in friction between the robot and the actual inner wall of the pipe is expected, which will improve the speed and stability of the snake robot.

4.2. Simulation of spiral motion

4.2.1. Parameter setting

Due to the current limitations of the hardware on our snake robot prototype in the laboratory, we are unable to perform experiments involving spiral motion. Therefore, we use the Adams simulation software to verify the accuracy of our model. We import the 3D model of the snake robot prototype designed to inspect the inner wall of pipelines into the Adams simulation software. We set specific material and contact parameters based on the laboratory environment and the experimental prototype. The key parameters are shown in Fig. 14. Next, we add fixed and revolute parts to the discrete joints of the snake robot. The rotation of the joint angles is controlled by the calculated joint angle function, allowing us to simulate a 3D spiral motion on the inner wall of a pipeline with a diameter of 300 mm. Because the Adams software is influenced by a function at time $t = 0$ s, it undergoes a direct transition from a value of zero to the angle value at $t = 0$ s. To prevent the solver from converging, a control function for spline fitting is employed to control the rotation of the joint (Fig. 15).

4.2.2. Results and analysis

The results of simulation experiments show that controlling the snake robot according to the joint angles calculated from the helical motion model in this paper can realize three-dimensional cylindrical helical motions with corresponding pitches in the inner wall of pipes with different pipe diameters.

Fig. 16 indicates that the helical motion of the snake robot occurs in accordance with the cylindrical helix curve based on the provided helix radius r and pitch h . By slightly increasing the helix radius r , the force exerted on the snake robot against the inner wall of the pipeline can be enhanced, leading to a

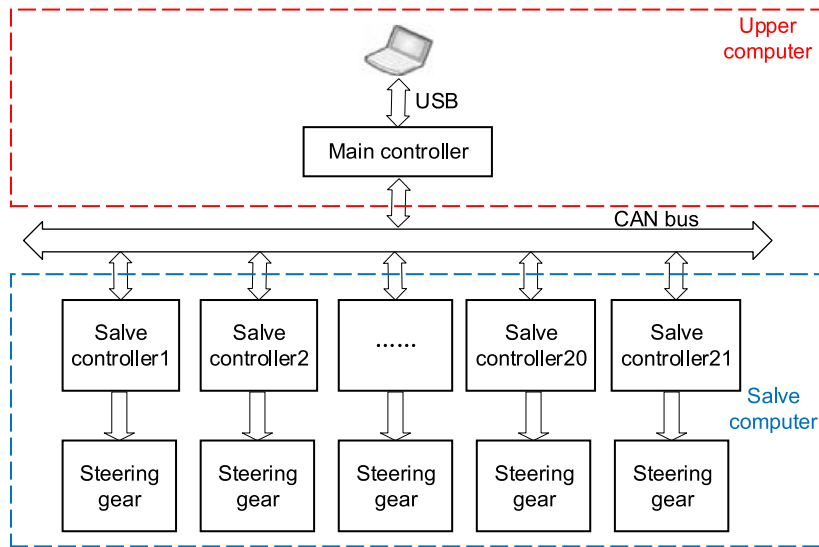


Fig. 12. Control system framework.

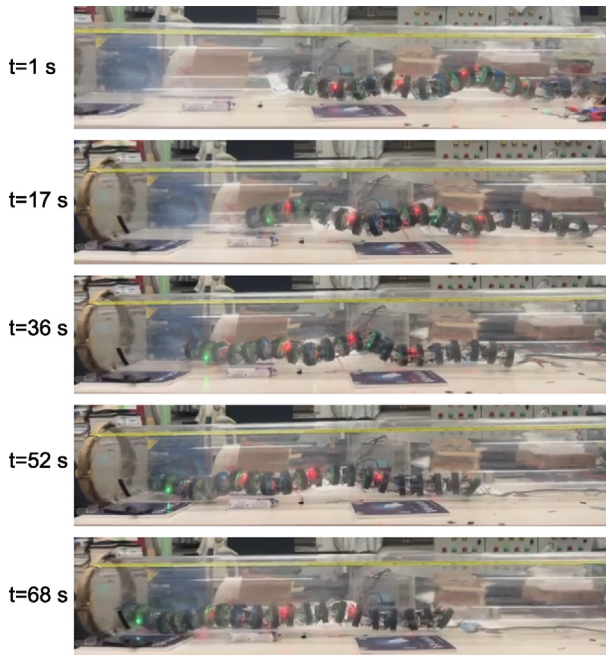


Fig. 13. Snake robot traveling wave motion in pipeline.

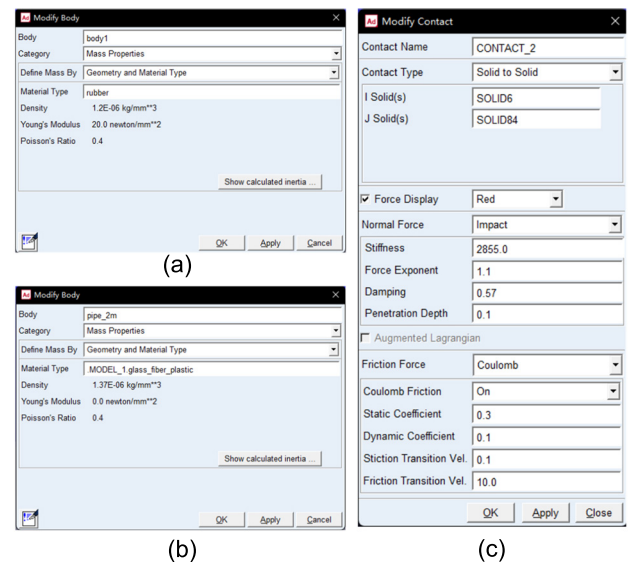


Fig. 14. Material and contact parameter setting. (a) Skin material parameters. (b) Laboratory pipe material parameters. (c) Contact parameters.

more stable state. Reducing the pitch h allows the snake robot to cover a larger area, resulting in more comprehensive inspection information. Nevertheless, it is important to note that the pitch h should not be too small during the cylindrical helix movement so as to prevent any collisions caused by the joint size of the snake robot.

Given the specified parameters of the conical spiral curve, the snake robot adopts a conical spiral shape with a decreasing spiral radius (Fig. 17). When the conical spiral motion occurs within a pipe with a fixed diameter, the robot's movement pattern allows a portion of the robot to detach from the pipe wall, thereby expanding its available space for movement. Additionally, conical spiral motion with an increasing radius can also be achieved by adjusting the joint angles, thereby providing a theoretical foundation for the development of a new type of three-dimensional spiral motion for snake robots.

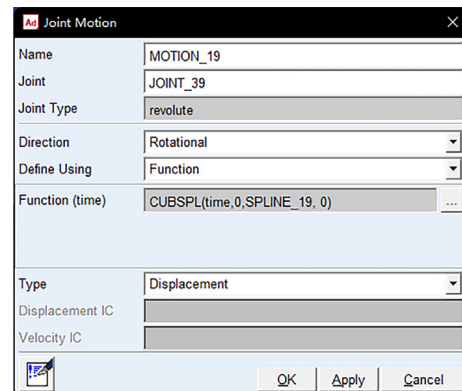


Fig. 15. Parameter settings for revolute motion.

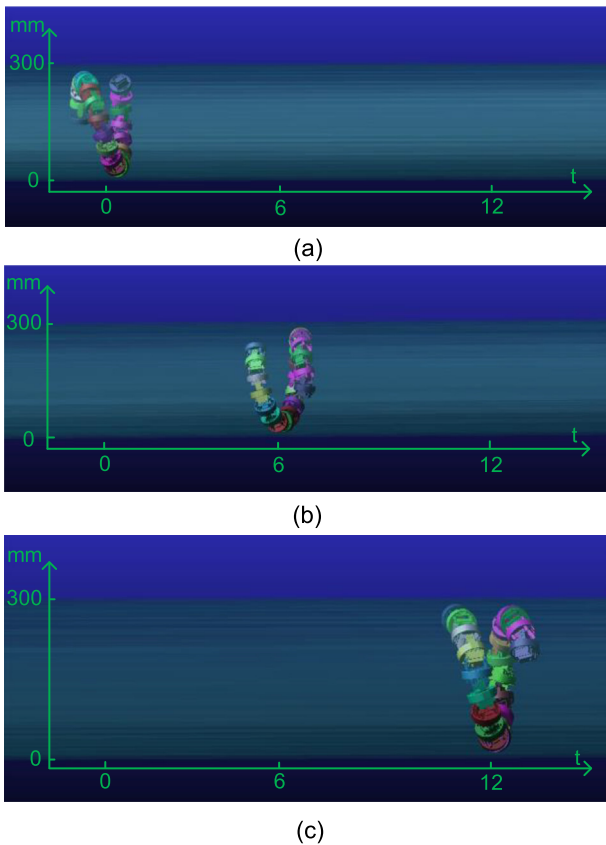


Fig. 16. The cylindrical helical gait of snake robot in pipeline. (a) Position and pose of snake shaped robot at $t = 0$ s. (b) Position and pose of snake shaped robot at $t = 6$ s. (c) Position and pose of snake shaped robot at $t = 12$ s.

5. Conclusions

In this study, we first complete the overall structural design of the snake robot prototype, and then establish simple undulatory and traveling wave motion control functions using the gait equation method. Subsequently, we apply the backbone curve method to calculate the joint angles of a discrete-structure snake robot during complex three-dimensional helical motion, and we model and derive the cylindrical and conical helices within three-dimensional helical lines. The models proposed in this study provide a more intuitive description of the physical significance of parameters within joint angle functions during cylindrical and conical helical motions.

We propose two specific motion models for the conical helical motion of discrete-structure snake robots: the equal-angle conical helix and the equal-pitch conical helix. Positioning the robot’s forward section in a conical helical state allows the camera to be centrally located along the pipeline axis to capture forward video image data, which is crucial for subsequent motion guidance. This also expands the variety of helical curves that snake robots can emulate, and the novel gait enables the robot to have greater maneuverability within pipes, showing excellent application prospects.

Physical and simulation experiments demonstrate that the snake robot can complete the corresponding motion gaits in both real pipes and virtual digital pipeline environments. Although conical spiral motion involves a more complex calculation process, by varying parameters, the robot can be controlled to execute spiral motions with gradually changing radii to obtain more activity space, paving the way for the development of more

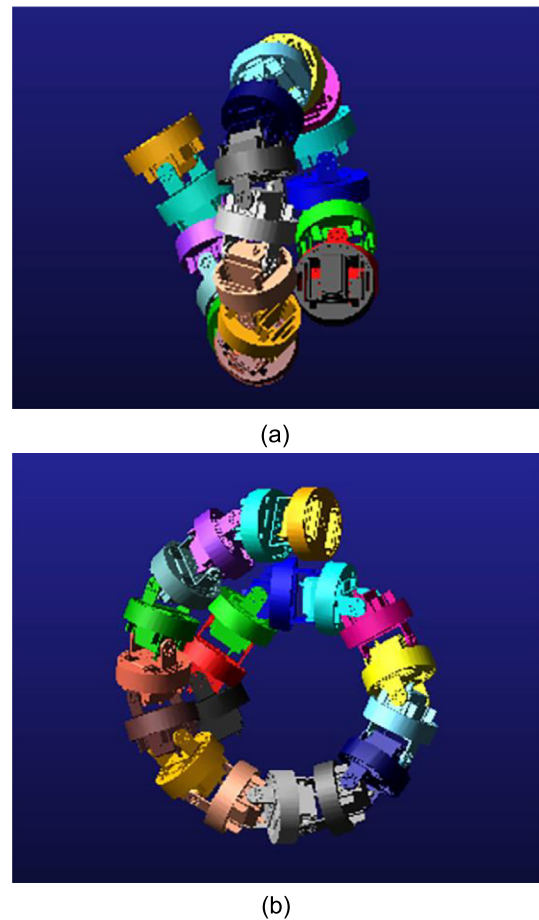


Fig. 17. The snake robot exhibits a conical spiral gait. (a) XOZ plane. (b) YOZ plane.

advanced gaits to achieve better motion effects or applications in various fields.

However, the control of various motion gaits is currently performed by directly applying theoretical joint angles without a corresponding negative feedback loop to enhance the overall motion robustness. In the future, we plan to design more effective negative feedback regulators for traveling waves and complex helical motions to achieve greater stability and robustness. Ultimately, our goal is to realize an engineering-level snake robot for pipeline inner wall inspection that is ready for practical application.

Declaration of competing interest

The authors declare that they have no known competing financial interests or personal relationships that could have appeared to influence the work reported in this paper.

Acknowledgment

This work was supported by the BUCEA Post Graduate Innovation Project, China (PG2023096).

Appendix A. Supplementary data

Supplementary material related to this article can be found online at <https://doi.org/10.1016/j.birob.2024.100156>.

References

- [1] X. Wang, Y. Wang, C. Zhang, Snake robot localization algorithm for pipeline detection based on inertial navigation, *Instrum. Tech. Sensor* (84–89) (2023).
- [2] D. Zhao, Y. Wang, L. Chen, A crack video detection system of pipeline snake shaped robot, *Sci. Technol. Eng.* 23 (6) (2023).
- [3] L.X. Rui Deng, Modeling simulation and experimental research on a snake shaped robot for pipeline detection, *Small Microcomput. Syst.* 42 (2496–2500) (2021).
- [4] T. Owen, *Biologically inspired robots: Snake-like locomotors and manipulators by shigeo Hirose* Oxford University Press, Oxford, 1993, 220pages, incl. index (£ 40), *Robotica* 12 (3) (1994) 282–282.
- [5] S. Ma, Analysis of snake movement forms for realization of snake-like robots, in: *Proceedings 1999 IEEE International Conference on Robotics and Automation (Cat. No. 99CH36288C)*, Vol. 4, IEEE, 1999, pp. 3007–3013.
- [6] M. Tesch, K. Lipkin, I. Brown, R. Hatton, A. Peck, J. Rembisz, H. Choset, Parameterized and scripted gaits for modular snake robots, *Adv. Robot.* 23 (9) (2009) 1131–1158.
- [7] D. Rollinson, H. Choset, Pipe network locomotion with a snake robot, *J. Field Robotics* 33 (3) (2016) 322–336.
- [8] B. Chong, T. Wang, J.M. Rieser, B. Lin, A. Kaba, G. Blekherman, H. Choset, D.I. Goldman, Frequency modulation of body waves to improve performance of sidewinding robots, *Int. J. Robot. Res.* 40 (12–14) (2021) 1547–1562.
- [9] P. Liljebäck, K.Y. Pettersen, Ø. Stavdahl, J.T. Gravdahl, Experimental investigation of obstacle-aided locomotion with a snake robot, *IEEE Trans. Robot.* 27 (4) (2011) 792–800.
- [10] G.S. Chirikjian, J.W. Burdick, A modal approach to hyper-redundant manipulator kinematics, *IEEE Trans. Robot. Autom.* 10 (3) (1994) 343–354.
- [11] H. Yamada, S. Hirose, Study on the 3D shape of active cord mechanism, in: *Proceedings 2006 IEEE International Conference on Robotics and Automation, 2006, ICRA 2006, IEEE, 2006*, pp. 2890–2895.
- [12] S.B. Andersson, Discretization of a continuous curve, *IEEE Trans. Robot.* 24 (2) (2008) 456–461.
- [13] P. Liljebäck, K.Y. Pettersen, Ø. Stavdahl, J.T. Gravdahl, A 3D motion planning framework for snake robots, in: *2014 IEEE/RSJ International Conference on Intelligent Robots and Systems, IEEE, 2014*, pp. 1100–1107.
- [14] B. Chong, Y. Ozkan Aydin, G. Sartoretto, J.M. Rieser, C. Gong, H. Xing, H. Choset, D.I. Goldman, A hierarchical geometric framework to design locomotive gaits for highly articulated robots, in: *Robotics: Science and Systems, 2019*.
- [15] W. Huang, X. Guo, H. Liu, Y. Fang, A robust model-based radius estimation approach for helical climbing motion of snake robots, *IEEE/ASME Trans. Mechatronics* (2023).
- [16] W. Zhen, C. Gong, H. Choset, Modeling rolling gaits of a snake robot, in: *2015 IEEE International Conference on Robotics and Automation, ICRA, IEEE, 2015*, pp. 3741–3746.
- [17] M. Inazawa, T. Takemori, M. Tanaka, F. Matsuno, Unified approach to the motion design for a snake robot negotiating complicated pipe structures, *Front. Robot. AI* 8 (2021) 629368.
- [18] Q. Ruan, J. Wu, Y.-a. Yao, Design and analysis of a multi-legged robot with pitch adjustable units, *Chin. J. Mech. Eng.* 34 (1) (2021) 64.
- [19] W. An, J. Wei, X. Lu, J.S. Dai, Y. Li, Geometric design-based dimensional synthesis of a novel metamorphic multi-fingered hand with maximal workspace, *Chin. J. Mech. Eng.* 34 (1) (2021) 41.
- [20] S.Y. Junhao Zhang, Snake robotics: Bionic mechanism, structure, actuation, modeling and control, *J. Mech. Eng.* 58 (75–92) (2022).
- [21] M. Moattari, M.A. Bagherzadeh, Flexible snake robot: Design and implementation, in: *2013 3rd Joint Conference of AI & Robotics and 5th RoboCup Iran Open International Symposium, IEEE, 2013*, pp. 1–5.
- [22] M. Saito, M. Fukaya, T. Iwasaki, et al., Modeling, analysis, and synthesis of serpentine locomotion with a multilink robotic snake, *IEEE Control Syst. Mag.* 22 (1) (2002) 64–81.
- [23] G.S. Chirikjian, J.W. Burdick, The kinematics of hyper-redundant robot locomotion, *IEEE Trans. Robot. Autom.* 11 (6) (1995) 781–793.
- [24] H. Yamada, S. Hirose, Approximations to continuous curves of active cord mechanism made of arc-shaped joints or double joints, in: *2010 IEEE International Conference on Robotics and Automation, IEEE, 2010*, pp. 703–708.
- [25] D. Xia, The geometric characteristics and drawing method of conical spiral with equal inclination angle and variable pitch, *J. Hefei Univ. Technol.: Natural Sci.* 15 (4) (1992) 138–144.